Available online at www.sciencedirect.com
SCIENCE DIRECT®
Computers & Fluids 33 (2004) 917–926
computers & fluids
www.elsevier.com/locate/compfluid

Assessment of sharp- and continuous-interface methods for drop in static equilibrium

Tao Ye, Wei Shyy *, Cheng-Feng Tai, Jacob N. Chung

Department of Mechanical and Aerospace Engineering, University of Florida, Gainesville, FL 32611-6250, USA

Received 4 December 2002; received in revised form 21 July 2003; accepted 16 August 2003

Abstract

Among the successful approaches for treating multiphase problems involving an interface, the continuous-interface method often handles the surface force via a locally integrated body force formulation. On the other hand, the sharp-interface method treats each phase separately while coordinating them via an explicit interface treatment. The sharp interface method computationally more demanding, but the continuous interface method can create spurious velocity in the interface region, which compromises the solution accuracy. Furthermore, the large property jumps often observed between liquid and vapor phases can influence the numerical accuracy, and needs to be investigated. In order to quantitatively demonstrate the relative performance of the sharp- and continuous-interface methods, we have considered a spherical drop in static equilibrium to highlight the role of the interface treatment. It is shown that the sharp-interface method is second-order accurate while the continuous-interface method is first-order. Furthermore, the sharp interface method is insensitive to the property jumps.

1. Introduction

Numerous techniques have been developed for tracking interfaces between separating materials, phases and properties. Categorically, there are moving grid (Lagrangian) [1–3] and fixed grid (Eulerian) approaches [4–6]. In the fixed grid approach, one can resort to the purely Eulerian approach such as the volume of fluid method [5] for free surface flows, or the enthalpy formulation [6,7] when phase change is involved. In these methods, the interface is constructed after the field solution is obtained. In the purely Eulerian approach, the interface construction is decoupled

* Corresponding author. Tel.: +1-352-392-0961; fax: +1-352-392-7303.
E-mail address: wss@mae.ufl.edu (W. Shyy).

0045-7930/$ - see front matter © 2003 Elsevier Ltd. All rights reserved.
doi:10.1016/j.compfluid.2003.08.002

from the field equation solver, which can cause difficulties such as uniqueness of the shape interpretation, and continuity and smoothness of the interface.

Alternatively, one can also explicitly track the interface utilizing the fixed grid but with additional procedures. The continuous interface method (CIM), such as the immersed boundary technique [8] or the level set method [9], has been popular. CIM defines the interface as part of the solution and can be conveniently coupled with the field equations. With this approach, the interface is of finite thickness, which reduces the order of accuracy of the overall solution to first-order [10,11], or even lower. For example, the spurious velocity field can result from such computations.

In addition to these techniques, the sharp interface method (SIM) has been developed in the last several years [12–15]. In SIM, the interface is considered to be a discontinuity separating two materials, with the field equations handled by the fixed grid, while directly accounting for the presence of the interface by forming irregularly shaped computational cells. At the modeling level, SIM is consistent with the concept of continuum mechanics because there is no smearing at the interface. As demonstrated in [16] for the fixed geometry problems, and in [14] for one-dimensional moving boundary problems, such approach exhibits higher order of accuracy than CIM. However, for cases involving curved free boundaries, no rigorous investigation of the performance of the sharp interface method has been performed.

In this report, we assess the performance of the sharp interface method recently developed by Ye et al. [15], using the spherical drop under static equilibrium as the test problem. This test problem has an analytical solution, and has been studied in detail for CIM [11,10]. It should be pointed out numerous studies have been published in the literature in regard to interfacial dynamics and multiphase flows involving complex physics, e.g., [14,15,17,18] and references cited therein. These problems include drop and bubble dynamics under various Webber, Reynolds and capillary numbers, and exhibit rich physical patterns according to the interplay between these parameters. However, because of the convection, buoyancy, viscous and unsteady effects, the accuracy of the treatment of the interfacial dynamics is often difficult to assess. As documented in detail by Kothe et al. [18] and by Lörstad et al. [17], substantial spurious velocity can arise in the interfacial region. Such spurious velocities can be masked in situations involving other mechanisms, making it difficult to trace the source of numerical inaccuracy for multiphase flow computations. It is with this background that we focus on a seemingly simple problem, which has been demonstrated to be difficult to handle computationally.

2. Governing equations and numerical procedure

The present sharp-interface method employs a combined Eulerian–Lagrangian strategy. As discussed in details in Ref. [15], the present SIM has the following distinguishing features:

(1) The finite-volume method is adopted to ensure the conservation of mass, momentum and energy transport in each phase/material.
(2) Specific governing equations are constructed for each phases/materials, instead of using the single set of governing equations for the entire domain of all phases/materials. This enables

the method to handle large property (such as density) ratios across the interface with relative ease.
(3) Sharp-interface with no numerical smearing.
(4) Interfacial constraints are imposed as the distinct boundary conditions, instead of being incorporated through source terms in the governing equations.
(5) The C^2 cubic B-spline curve fitting method is employed to represent the interface. A fairing algorithm for curvature calculation makes it possible to use the current SIM to compute problems in which accurate curvature estimation is critical for simulating interfacial dynamics.

In addition, the present method also has the capability to treat the phase change at the interface. An illustration of the cell and interface intersection treated in the sharp interface method [14–16] is depicted in Fig. 1. It is noted that the small fragments of cut-cells are absorbed into the neighboring cells in the same phase to form larger, trapezoid cells. In the present approach, the interface, represented by suitable geometric representations based on massless markers, intersects with the underlying, fixed Cartesian grid. A compact interpolation method near the interface is adopted to retain second-order accuracy and conservation property. The smoothness of the interfacial curve, especially in regard to the curvature, is handled with the aid of a curve-fairing algorithm [19].

For the equilibrium drop problem, two sets of equations are solved separately in the two phases. Assuming constant properties, the mass and momentum equations in liquid and gas phases are as follows:

Liquid-phase equations (the drop)

$$\begin{aligned} &\nabla \cdot \boldsymbol{u}_{\mathrm{l}} = 0 \\ &\rho_{\mathrm{l}}\left[\frac{\partial \boldsymbol{u}_{\mathrm{l}}}{\partial t} + \nabla \cdot (\boldsymbol{u}_{\mathrm{l}}\boldsymbol{u}_{\mathrm{l}})\right] = -\nabla p_{\mathrm{l}} + \nabla \cdot (\mu_{\mathrm{l}} \nabla \boldsymbol{u}_{\mathrm{l}}) \end{aligned} \tag{1}$$

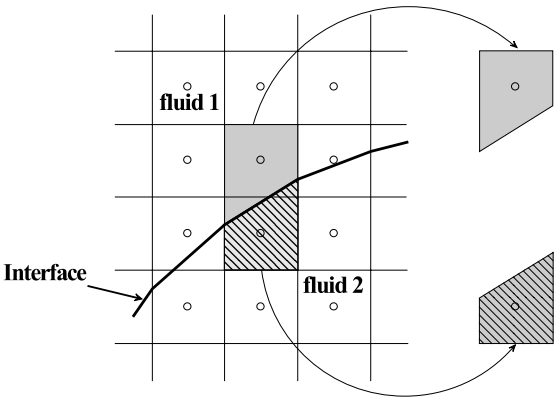

Fig. 1. Illustration of the cell-interface intersection in the sharp interface method. Trapezoidal cells are formed near the interface.

Gas-phase equations (surrounding fluid)

$$\nabla \cdot \boldsymbol{u}_{\mathrm{v}} = 0$$
$$\rho_{\mathrm{v}}\left[\frac{\partial \boldsymbol{u}_{\mathrm{v}}}{\partial t} + \nabla \cdot (\boldsymbol{u}_{\mathrm{v}}\boldsymbol{u}_{\mathrm{v}})\right] = -\nabla p_{\mathrm{v}} + \nabla \cdot (\mu_{\mathrm{v}} \nabla \boldsymbol{u}_{\mathrm{v}}) \tag{2}$$

where subscript 'l', 'v' denotes the liquid and gas phase, respectively; ρ is density, μ is viscosity. The variable property as well as additional transport mechanisms, such as energy equation, can be directly incorporated. These conditions are not considered here.

On the interface, several conditions need to be satisfied; they are met via an iterative process coupled with the flow field solutions.

Mass flux continuity on interface

$$\dot{m} = \rho_{\mathrm{l}}(u_{\mathrm{int}} - u_{\mathrm{l}}) \cdot n = \rho_{\mathrm{v}}(u_{\mathrm{int}} - u_{\mathrm{v}}) \cdot n \tag{3}$$

Here, $\dot{m}$ is the interfacial mass flux; ρ_{l}, ρ_{v} present the density in liquid and vapor phase; n is the unit normal vector at interface; u_{int}, u_{l}, u_{v} are the velocity of interface, liquid phase and vapor phase, respectively.

Force balance on interface

$$\rho_{\mathrm{v}}[(u_n)_{\mathrm{v}} - (u_n)_{\mathrm{int}}] \cdot u_{\mathrm{v}} + p_{\mathrm{v}} \cdot n - \tau_{\mathrm{v}} \cdot n = \rho_{\mathrm{l}}[(u_n)_{\mathrm{l}} - (u_n)_{\mathrm{int}}] \cdot u_{\mathrm{l}} + p_{\mathrm{l}} \cdot n - \tau_{\mathrm{l}} \cdot n + \sigma\kappa n \tag{4}$$

where, τ_{l}, τ_{v} presents the viscous stress tensor in liquid and vapor phase; σ is the surface tension coefficient; κ is the curvature of the interface; p_{l}, p_{v} are the pressure in liquid and vapor phase; $(u_n)_{\mathrm{v}}$, $(u_n)_{\mathrm{l}}$, $(u_n)_{\mathrm{int}}$ mean the velocity of vapor phase, liquid phase at the interface in normal direction and the interface velocity in the normal direction.

3. Results and discussion

For the present test problem, the density ratio $\rho_{\mathrm{l}}/\rho_{\mathrm{v}}$ between the liquid drop and surrounding gas varies from 1 to 1000. The largest ratio corresponds to the circumstance between water and air under the standard atmospheric condition. With a spherical drop in static equilibrium, there are two uniform pressure fields inside and outside of the drop boundary, namely, the pressure inside is $p_0 + \frac{2\sigma}{R}$ and outside is p_0. The difference balances the surface tension effect, according to the Young–Laplace condition [7].

$$\Delta p_{\mathrm{exact}} = \frac{2\sigma}{R} \tag{5}$$

where σ is the surface tension and R is the radius of the droplet. In the present study, σ is set to 1.0 N/m and R equals to 0.25 m; the exact pressure difference $\Delta p_{\mathrm{exact}}$, therefore, should be equal to 8.0 N/m^2. The numerical result of the pressure difference is compared against this exact value.

In the present study, the drop is located at the center of a circular cylinder. Both the height and the diameter of the cylinder are twice the drop diameter. Given axi-symmetric nature of the problem, only half of the computational domain is considered, with the bottom boundary being the symmetric axis. On other boundaries of the domain, zero viscous stress conditions are

specified for velocity field and the zero gradient condition is adopted for pressure. A fixed, uniform Cartesian grid is employed. The initial condition consists of constant pressure in the entire domain, with different density values assigned inside and outside of the drop. The solutions are obtained by solving the mass continuity and momentum equations, Eqs. (1) and (2), along with the interfacial conditions, Eqs. (3) and (4). A numerical procedure for simultaneously solving flow fields, and satisfying momentum jump at the interface and mass conservation in each phase is carefully designed.

The case with a density ratio of 1000 is considered first. Unless noted otherwise, the ratio of the drop radius to the grid size, $R/\Delta x$, is 50, namely, with 100×200 grid (along radial and longitudinal directions, respectively) covering the entire computational domain. Fig. 2 shows the pressure distribution and velocity vectors (with all vectors set to be of the unit magnitude) in the domain. Detailed profiles along both horizontal and vertical directions are shown in Fig. 3. Figs. 2 and 3 demonstrate that the sharp interface method with the cut-cell treatment can capture the crisp pressure distribution across the interface. Fig. 4 depicts the profiles of the velocity components in

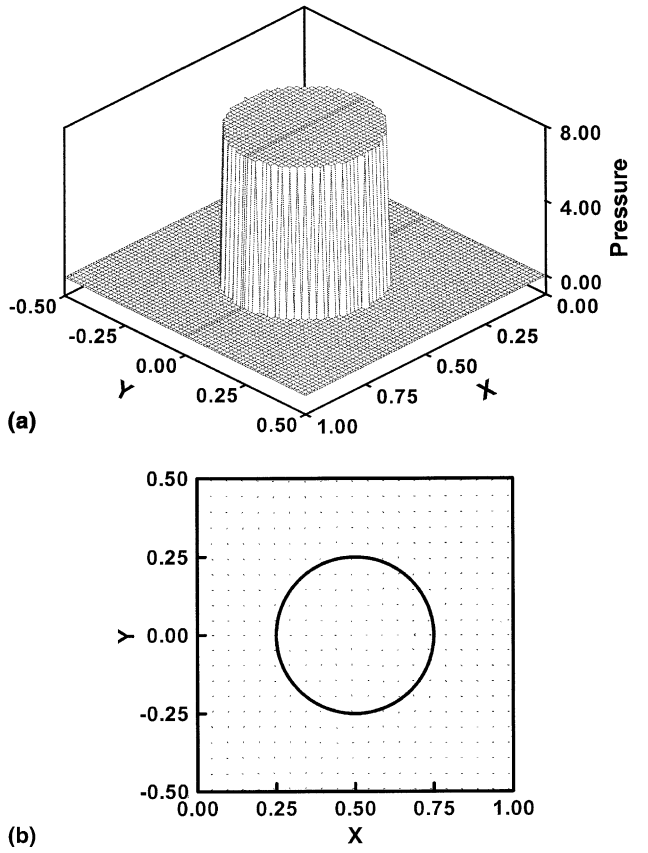

Fig. 2. The overall pressure and velocity distributions for a drop in static equilibrium (a) pressure, (b) velocity vectors. The maximum values of the u- and v-component of the spurious velocity are 4.687×10^{-10} and 4.279×10^{-10}, respectively.

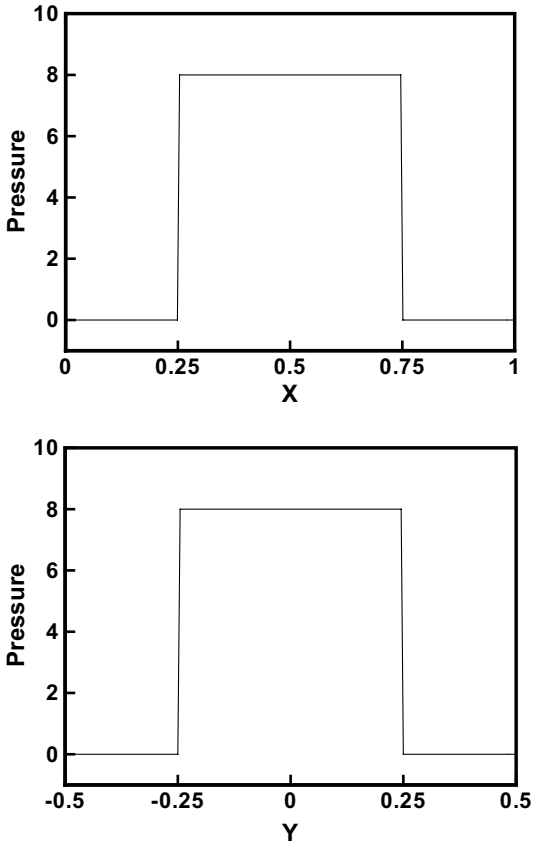

Fig. 3. Pressure profiles along the horizontal and vertical center lines.

both x and y directions. In contrast to CIM (see, e.g. [18]), which typically yields substantial spurious velocity, SIM produces errors virtually at the round-off level.

The curvature computation is a key in many interfacial transport problems; they are also very difficult to compute accurately because of the non-linear combination of first and second derivatives. To assess the performance of SIM, Fig. 5 presents the computed curvature, plotted along the entire circumference of the drop boundary. Accurate estimation has been obtained with little noise associated with the result.

Next, we assess the order of accuracy of the SIM solution. The assessment is based on the overall pressure difference, defined as:

$$\Delta p_{\text{num}} = \frac{1}{N_{\text{in}}} \sum_{n=1}^{N_{\text{in}}} P_n - \frac{1}{N_{\text{out}}} \sum_{n=1}^{N_{\text{out}}} P_n \tag{6}$$

where, N_{in} is the number of cells inside the bubble and N_{out} is the cells outside; p_n is the pressure in each cell. In Fig. 6 and Table 1, the solutions of SIM and CIM (using the immersed boundary method) are compared with varying grid size, Δx. The relative error between the theoretical and

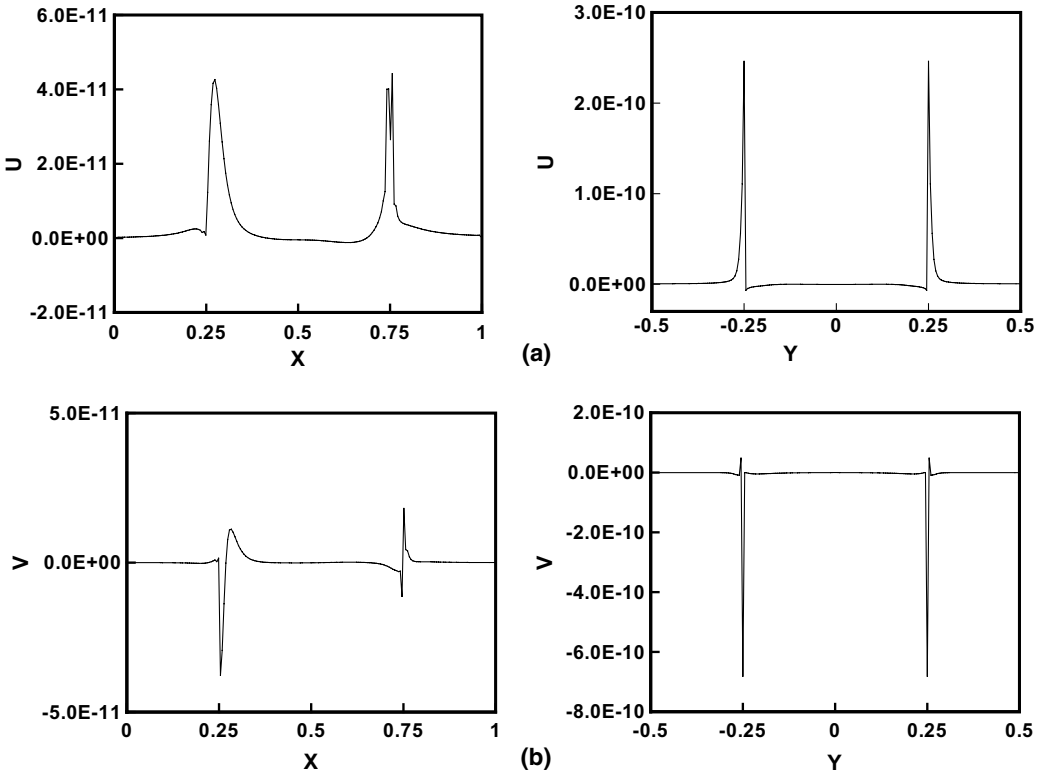

Fig. 4. Velocity profiles along the horizontal and vertical center lines. (a) horizontal-velocity component, (b) vertical-velocity component.

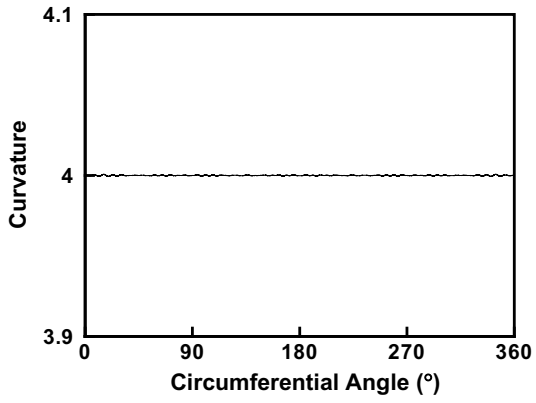

Fig. 5. The computed curvature along the circumference of the drop interface, from 0° to 360°.

numerical pressure difference can be expressed in terms of L_2-norm. L_2-norm of the error was defined as:

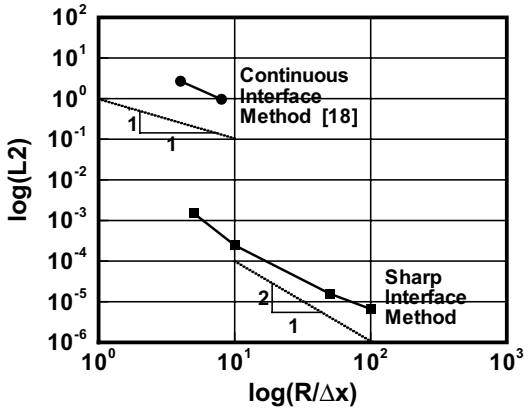

Fig. 6. Comparison between the sharp and continuous interface methods based on the error norms defined in Eq. (7).

Table 1
Effect of the grid size for a spherical drop in static equilibrium

$R/\Delta x$	ρ_l/ρ_v	$\Delta p_{num}/\Delta p_{exact}$	Pressure error norm L_{2B}
5	1000.0	0.9988	1.509E−03
10	1000.0	0.9998	2.452E−04
50	1000.0	1.000	1.612E−05
100	1000.0	1.000	6.632E−06

$$L_{2B} = \sqrt{\frac{1}{N_{in}} \sum_{n=1}^{N_{in}} \frac{(P_{num} - P_{exact})^2}{P_{exact}^2}} \tag{7}$$

Fig. 6 and Table 1 confirm that SIM offers noticeably lower error with approximately overall second-order accuracy. For comparison purpose, representative results based on the CIM [18] are also depicted in Fig. 6; it yields first-order accuracy and the errors are several orders of magnitude larger for all grid resolutions.

Finally, we assess the effect of the density ratio, between drop and surrounding gas, on the computational accuracy. Table 2 presents the pressure error norm, defined by Eq. (7), for density ratios of 1, 10, 100 and 1000, with the same spatial resolution. There is little sensitivity of the SIM performance with respect to the density effect, which, again, is not the case for CIM.

Table 2
Effect of the density ratio on the spurious velocity and pressure fields for a spherical drop in static equilibrium

$R/\Delta x$	ρ_l/ρ_v	u_{max}	v_{max}	Pressure error norm L_{2B}
50	1.0	4.816E−10	4.612E−10	1.607E−005
50	10.0	4.686E−10	4.277E−10	1.607E−005
50	100.0	4.686E−10	4.279E−10	1.608E−005
50	1000.0	4.687E−10	4.279E−10	1.612E−005

In conclusion, the SIM is effective and accurate in resolving interfacial characteristics, including hydrodynamic variables and geometric information. It is more demanding computationally because the field equations in each phase need to be coupled between different materials/phases, and explicitly linked with the interfacial conditions. For detailed information related to the CIM, including the number of iteration, the coordination between phases and the interface, and the CPU time, we refer to our previous work [15,16]. In return, second-order accuracy is achieved as compared to the first-order accuracy in CIM, indicating that the SIM can handle more complicated problems requiring higher accuracy.

Acknowledgement

The present research is supported by NASA under the URETI program.

References

[1] Ryskin G, Leal LG. Numerical solution of free boundary problems in fluid mechanics, Part I, II, III. J Fluid Mech 1984;148:1–43.
[2] Harlow FH, Welch JE. Numerical calculation of time-dependent viscous incompressible flow of fluid with free surface. Phys Fluids 1965;8:2182–9.
[3] Vicelli JA. A method for including arbitrary external boundaries in the MAC incompressible fluid computing technique. J Comput Phys 1969;4:543–51.
[4] Peskin CS. Numerical analysis of blood flow in the heart. J Comput Phys 1977;25:220–52.
[5] Hirt CW, Nichols BD. Volume of fluid (VOF) method for the dynamics of free boundaries. J Comput Phys 1981;39:201–25.
[6] Shyy W, Udaykumar HS, Rao MM, Smith RW. Computational Fluid Dynamics with Moving Boundaries. Washington, DC: Hemisphere; 1996.
[7] Shyy W. Computational Modeling for Fluid Flow and Interfacial Transport. Amsterdam, Netherlands: Elsevier; 1994.
[8] Shyy W, Francois M, Udaykumar HS, N'dri N, Tran-Son-Tay R. Moving boundaries in micro-scale biofluid dynamics. Appl Mech Rev 2001;54(5):405–53.
[9] Osher S, Sethian JA. Fronts propagating with curvature dependent speed: algorithms based on Hamilton–Jocobi formulations. J Comput Phys 1988;79:12–49.
[10] Francois M, Shyy W. Micro-scale drop dynamics for heat transfer enhancement. Progr Aerospace Sci 2002;38:275–304.
[11] Williams MW, Kothe DB, Puckett EG. Accuracy and convergence of continuum surface-tension models. In: Shyy W, Narayanan R, editors. Fluid Dynamics At Interfaces. New York: Cambridge University Press; 1999.
[12] LeVeque RJ, Li Z. The immersed interface method for elliptic equations with discontinuous coefficients and singular sources. SIAM J Numer Anal 1994;31(4):1019.
[13] Udaykumar HS, Shyy W, Rao MM. ELAFINT: a mixed, Eulerian–Lagrangian method for fluid flows with complex and moving boundaries. Int J Numer Meth Fluids 1996;22:691–712.
[14] Udaykumar HS, Mittal R, Shyy W. Computation of solid–liquid phase fronts in the sharp interface limit on fixed grids. J Comput Phys 1999;153:535–74.
[15] Ye T, Shyy W, Chung JN. A fixed-grid, sharp-interface method for bubble dynamics and phase change. J Comput Phys 2001;174:781–815.
[16] Ye T, Mittal R, Udaykumar HS, Shyy W. An accurate cartesian grid method for viscous incompressible flows with complex immersed boundaries. J Comput Phys 1999;156:209–40.

[17] Lörstad D, Francois M, Shyy W, Fuchs L. Assessment of volume of fluid and immersed boundary methods for droplet computations, AIAA Paper No. 2003-1282, 2003.
[18] Kothe DB, Rider WJ, Mosso SJ, Brock JS, Hochstein JI. volume tracking of interfaces having surface tension in two and three dimensions, AIAA paper 96-0859, 1996.
[19] Farin G. Curves and Surface for Computer-Aided Geometric Design, A Practical Guide. 4 ed. Academic Press; 1997.